



Site-selective Pt dewetting on WO_3 -coated TiO_2 nanotube arrays: An electron transfer cascade-based H_2 evolution photocatalyst



Davide Spanu^{a,b}, Sandro Recchia^b, Shiva Mohajernia^a, Patrik Schmuki^{a,c,*}, Marco Altomare^{a,*}

^a Department of Materials Science and Engineering WW4-LKO, University of Erlangen-Nuremberg, Martensstrasse 7, D-91058 Erlangen, Germany

^b Department of Science and High Technology, University of Insubria, via Valleggio 11, 22100 Como, Italy

^c Chemistry Department, Faculty of Sciences, King Abdulaziz University, 80203 Jeddah, Kingdom of Saudi Arabia

ARTICLE INFO

Keywords:
 Anodic TiO_2 nanotubes
 Pt dewetting
 WO_3
 Photocatalytic H_2 generation
 Charge transfer
 Electron transfer cascade

ABSTRACT

Among several parameters that affect the yield of a photocatalytic process mediated by a metal oxide semiconductor, key is the efficient separation and transfer of photo-generated charge carriers. To overcome kinetic limitations and enable charge transfer, an effective strategy is to decorate the photocatalyst surface with cocatalytic nanoparticles of either a second semiconductor metal oxide or a noble metal. Nevertheless, classical deposition techniques based on powder technology approaches lead to randomly placed cocatalytic nanoparticles at the photocatalytic surface. The poor control over cocatalyst placement can drastically hamper the photocatalytic efficiencies, and can also prevent a full understanding of the charge carrier dynamics and photocatalytic mechanism. Here we investigate a highly defined charge separation platform for photocatalytic H_2 evolution based on a Pt- WO_3 - TiO_2 “stacked” structure constructed on anodically grown TiO_2 nanotube arrays. Key is the formation of a site-selective and sequential W and Pt metal sputter-decoration only at the mouth of highly-ordered TiO_2 nanotubes. After placing the W-Pt bilayer at the nanotubes mouth, a suitable thermal treatment forms a WO_3 layer atop the nanotubes while the Pt film undergoes solid state dewetting into 2–6 nm-sized Pt nanoparticles. These structures show strongly improved photocatalytic H_2 evolution efficiency compared to any other single-cocatalyst system (Pt- TiO_2 and WO_3 - TiO_2) and pristine TiO_2 nanotubes. The photocatalytic activity improvement is ascribed to an enhanced charge carrier separation mechanism enabled by the well-defined TiO_2 - WO_3 -Pt architecture that provides swift electron transfer through WO_3 and towards Pt for H_2 evolution.

1. Introduction

Since the pioneering work of Fujishima and Honda [1] in 1972, the production of H_2 by photocatalytic splitting of H_2O on semiconductors has been extensively investigated. Among the different studied photocatalysts, titanium dioxide (TiO_2) received large attention owing to its suitable conduction (CB) and valence band (VB) edge positions, as well as for its nontoxicity and stability against corrosion and photo-corrosion [2,3]. The bottom of TiO_2 conduction band (CB) lies higher than the redox potential of water (-0.45 and 0 V vs. NHE, respectively, at pH 0) [4]. Therefore, by promoting electrons in TiO_2 CB through UV light irradiation (E_g TiO_2 \sim 3.0–3.2 eV), it is possible to reduce H_2O to H_2 .

However, pristine TiO_2 shows low efficiencies for H_2 production because of trapping and recombination of charge carriers, and owing to a kinetically slow electron transfer to reactants. Nanostructured photocatalysts can be employed in order to improve the electron transfer efficiency. Particularly, one-dimensional (1D) nanostructures, such as

anodic TiO_2 nanotubes (NTs), have attracted great attention in the last decades [5–7]. Vertically aligned arrays of self-organized NTs can be grown by a simple anodization of Ti metal in a suitable electrolyte [2,3,8]. The electrochemical conditions can be adjusted in order to lead to a large palette of nanotubular morphologies [8,9]. These highly-ordered 1D TiO_2 structures can promote directional charge transport and orthogonal electron-hole separation that allow for enhanced photoelectrochemical and photocatalytic performances [3,10].

In addition, cocatalysts that aid charge separation and transfer by forming a heterojunction on TiO_2 , such as a suitable semiconductor or noble metal nanoparticles (e.g. Au, Pd, Pt) can be also employed to further improve the performance of titania-based photocatalysts.

In view of constructing a composite photocatalyst, a particularly interesting constellation is obtained when TiO_2 is combined to WO_3 , an n-type semiconductor with a band gap E_g WO_3 \sim 2.6–2.8 eV [11,12]. With such a combination, a favorable band alignment at the TiO_2 - WO_3 interface is generated that enables efficient charge separation [13] by

* Corresponding authors at: Department of Materials Science and Engineering WW4-LKO, University of Erlangen-Nuremberg, Martensstrasse 7, D-91058 Erlangen, Germany.
 E-mail addresses: schmuki@ww.uni-erlangen.de (P. Schmuki), marco.altomare@fau.de (M. Altomare).

transfer of TiO_2 CB electrons into the WO_3 CB [14–17]. The photocatalytic enhancement obtained when WO_3 is combined to TiO_2 is frequently discussed in terms of WO_3 contribution to visible-light absorbance ($\lambda_{\text{abs, WO}_3} < \sim 450 \text{ nm}$ – i.e. larger photon harvesting) [18,19], enhanced surface acidity that can yield improved adsorption of reactants [20–25], higher hydrophilicity [26], and the possibility of enabling a “z-scheme” for charge separation [27].

While the placement of a suitable metal oxide semiconductor (WO_3) at the TiO_2 surface can enhance charge-separation, localized Schottky-type junctions are also commonly formed by placing noble metal cocatalytic nanoparticles on the individual oxides. For example, Pt is typically a most efficient cocatalyst for the H_2 generation reaction [28–31]. Pt nanoparticles at the TiO_2 surface can enable efficient electron transfer at the catalyst/environment interface by providing a favorable solid state junction to TiO_2 [4], hence improving the electron transfer to reactants while additionally catalyzing hydrogen atom recombination reaction, and thus facilitating H_2 gas formation ($2\text{H}^\circ \rightarrow \text{H}_2$) [32,33].

These two cocatalyst principles, i.e. a charge separation cocatalyst (WO_3) and a charge transfer cocatalyst (Pt), can, based on an anticipated synergistic effect, be combined into a composite photocatalyst, e.g. in a TiO_2 - WO_3 -noble metal combination. The benefit of combining these three catalytic elements has been used also in thermal catalysis, e.g. by using TiO_2 - WO_3 -Pt composites as de- NO_x catalysts [34].

In some recent studies, such as the work of Pap et al., TiO_2 - WO_3 -noble metal (Au, Pt) powders were investigated in view of their photocatalytic performance [35–38]. These works pointed out the potential of combining the two cocatalyst principles for efficient photocatalysis, but the chosen preparation method, based on a classical powder technology process, suffers from a poor control over morphology and stacking of the cocatalysts. Particularly, only a loose and undefined contact (junction) between the two oxides can be obtained – this hampers the charge carrier separation: note that in these works any noble metal- WO_3 - TiO_2 combination was found to be less photocatalytically active for H_2 evolution than a simple noble metal- TiO_2 configuration.

Moreover, similar synthesis methods for noble metal- WO_3 - TiO_2 structures lead in general to a photocatalyst configuration characterized by undefined interfaces, which can bring about an uncontrolled charge carried dynamics and various different photocatalytic mechanisms – in other words, given that a photocatalytic enhancement can be observed, an accurate understanding of the photocatalytic mechanism is almost impossible.

In contrast, with the present work, we introduce a defined and reliable fabrication strategy of a synergistic Pt- WO_3 - TiO_2 photocatalyst for H_2 generation constructed with nanoscale precision on an array of highly-ordered TiO_2 nanotubes. This architecture, owing to its highly-defined geometry obtained by site-selective placement of Pt and WO_3 cocatalysts, induces an electron transfer cascade from the TiO_2 NTs (light absorber) to the WO_3 junction (charge separation cocatalyst) and onward to the Pt nanoparticles (NPs) (charge transfer cocatalyst). The result is a facilitated electron transport towards the nanotube top for H_2 evolution, while the uncoated bottom of the TiO_2 cavities is a suitable site for hole-mediated oxidation reaction. We show that, in contrast to previous works, a morphologically controlled TiO_2 - WO_3 -Pt design leads to enhanced photocatalytic H_2 evolution efficiencies, which are higher than those measured for classic noble metal- TiO_2 photocatalysts.

2. Experimental

2.1. Fabrication of the TiO_2 nanotube array

Ti foils (Advent Research Materials, 0.125 mm thickness, 99.6% purity) were degreased by sonicating in acetone, ethanol, and deionized water, and were then dried in a N_2 stream. Then, the Ti foils were anodized to fabricate the highly ordered TiO_2 nanotube arrays in a hot

electrolyte based on 3 M HF in o- H_3PO_4 (Sigma-Aldrich) [39]. For the anodic growth, a two-electrode configuration was used, where the Ti foil (15 mm × 15 mm) and a Pt sheet were the working and counter electrodes, respectively. The anodization experiments were carried out by applying a potential of 15 V (for 2 h) using a DC power supply (VLP 2403 Voltcraft). After anodization, the TiO_2 nanotube arrays on Ti metal substrates were rinsed with ethanol and dried under N_2 stream.

2.2. W and Pt sputtering-coating and thermal treatment

In order to site-selectively place the cocatalytic Pt/ WO_3 stack only atop the nanotubes, a plasma-sputtering machine (EM SCD 500, Leica) was used in a shallow angle configuration to sputter-coat W and Pt metal thin films (W-Pt bilayers) using a 99.8% pure W target (Hauner Metallische Werkstoffe) and a 99.99% pure Pt target (Hauner Metallische Werkstoffe), respectively. The applied sputtering current was 16 mA and the pressure of the sputtering chamber was set at 10^{-2} mbar of Ar. The amount of sputtered material was in-situ determined by an automated quartz crystal monitor, and is reported in this work as nominal thickness of the sputtered film. In previous work the deposition process for Pt was calibrated, and a linear correlation was found between the nominal thickness of the sputtered layer (in nm) and the actual loading on the catalyst (in μg_{Pt}) [28,40]. The Pt loading determined by ICP-OES measurements scales with the nominal thickness of the sputtered layer with a factor of $1.1 \mu\text{g}_{\text{Pt}} \text{ nm}^{-1}$. In this work, the sputter-coated Pt films have a nominal thickness of 1 nm, and are coated on an active surface (irradiated photocatalyst surface) of 0.78 cm^2 . Thus, for Pt-leaded structures, the Pt loading is $\sim 1.4 \mu\text{g}_{\text{Pt}} \text{ cm}^{-2}$.

The Pt film nominal thickness of 1 nm was selected based on previous works demonstrating that a thickness of the sputter-coated noble metal film $< 5 \text{ nm}$ leads after dewetting to optimized cocatalyst loading and photocatalytic efficiency. In some cases, it was found that minimal amounts as low as e.g. 1 nm can lead to a highest H_2 evolution rate [28].

Subsequently, the samples were annealed at 450°C in air for 1 h, using a Rapid Thermal Annealer (Jipelec Jetfirst 100 RTA), with a heating and cooling rate of $30^\circ\text{C min}^{-1}$. The thermal treatment formed a WO_3 layer on the TiO_2 nanotube arrays onto which the Pt film splits into nanoparticles by thermal dewetting.

2.3. Characterization of the structures

A field-emission scanning electron microscope (FE-SEM, Hitachi S4800) and a high resolution transmission electron microscope (HR-TEM, Philips CM300) were used to characterize the morphology of the samples. Sample chemical composition analysis as well as valence band measurements were carried by X-ray photoelectron spectroscopy (XPS, PHI 5600, US). XPS spectra were acquired using Al X-ray source. The XPS spectra were corrected in relation to the Ti2p signal at 458.5 eV. PHI MultiPak™ software and database were used for quantitative analysis. X-ray diffraction (XRD) with an X'pert Philips MPD (equipped with a Panalytical X'celerator detector) was employed to examine the crystallographic properties of the materials. The light absorption properties (diffuse reflectance, DR) of the samples were measured by a UV-vis Spectrophotometer (Lambda 950, PerkinElmer).

2.4. Photocatalytic experiments

The photocatalytic H_2 generation measurements were carried out by irradiating the oxide films with UV light (LED Opsytec, $\lambda = 365 \text{ nm}$, beam size = 0.78 cm^2 , power of 80 mW cm^{-2}) in a 20 vol% ethanol–water solution (ethanol was used as hole-scavenger) in a quartz tube sealed with a gas-tight cap. The ethanol–water solution (kept under static conditions during the runs) and the cell head-space (volume = 6.22 mL) were purged with N_2 gas for 15 min prior to photocatalysis. N_2 -purging is needed as O_2 , if present, would reduce the

efficiency of H_2 generation by competitively reacting with conduction band electrons forming O_2^- .

The amount of produced H_2 (which was accumulated over the irradiation time in the head space of the tube) was measured by using a gas chromatograph (GCMSQO2010SE, Shimadzu) equipped with a thermal conductivity detector and a Restek micropacked Shin Carbon ST column (2 m \times 0.53 mm). GC measurements were carried out at a temperature of the oven of 45 °C (isothermal conditions), with the temperature of the injector set at 280 °C and that of the TCD fixed at 260 °C. The flow rate of the carrier gas, i.e., argon, was 14.3 mL min⁻¹. The majority of the experiments lasted 5 h, and the amount of evolved H_2 was measured at the end of the experiments. Photocatalytic measurements of Acid Orange 7 (AO7) degradation were carried out with the same instrumental setup and using a 0.125 mM AO7 solution. The light absorbance of the solution was measured by using a UV-vis spectrophotometer (Lambda XLS+, Perkin Elmer) at 485 nm wavelength (maximum absorbance value) in order to determine the AO7 concentration.

3. Results and discussion

Fig. 1a shows the morphology of the highly-ordered anodic TiO_2 NTs used in this work, which are grown on Ti metal foils by anodization in a hot H_3PO_4 /HF electrolyte [39]. These NTs have an almost ideal hexagonal packing, an average inner diameter of ~ 80 –90 nm and a length of ~ 190 –200 nm (see Inset in Fig. 1a). This well-defined structure with short aspect-ratio allows for the site-selective decoration of only the NT top, with e.g. metal bilayers (Pt and W in this work) using a grazing-angle sputtering technique.

After the sputter-deposition of a metal film, e.g. a 1 nm-thick Pt film, a thermal treatment is carried out to crystallize the TiO_2 NTs. Worth nothing, as illustrated in Fig. 1b, such a thermal treatment leads at the same time to solid state dewetting of Pt, that is, to the conversion of the sputtered Pt film into Pt nanoparticles, with spherical shape and average diameter of 2–6 nm (as shown in Fig. 1c and d). The driving

force for dewetting [41] is the minimization of the free surface energy of the metal (Pt) film, of the substrate (oxide surface) and of the metal–substrate interface (Pt/oxide). Since the thinner the metal film the higher its surface-to-volume ratio and thus its surface energy, the dewetting of e.g. few nm-thick metal films can occur also at temperature far below the metal melting point – that is, the film can dewet while remaining in the solid state [42].

The NT structures can also be decorated by sputtering a W film firstly (nominal thickness of 0–30 nm), followed by sputter-deposition of a thin Pt metal layer (nominal thickness of 1 nm) – i.e. using a sequential metal sputter-coating approach that form a W-Pt bilayer at the TiO_2 NT surface. A subsequent thermal treatment of these structures in air at 450 °C for 1 h forms the architectures illustrated in Fig. 2 (additional SEM images for these structures are reported in Fig. S1).

In the case of small amounts of shallow-angle sputtered W (nominal thickness < 10 nm, e.g. Fig. 2a and b), it is possible to observe from the cross-sectional SEM picture (Fig. 2b) that the deposition of the W film occurs only at the rim of the tubes, thus leaving the tube bottom uncovered (providing free TiO_2 surface). However, for thicker W films (≥ 10 nm, Fig. 2c and d) a certain amount of W is deposited also deep in the NTs – e.g. Fig. 2d shows that WO_3 is formed also close to the NT bottom.

The structures in Figs. 1 and 2 were characterized by XRD, HR-TEM in view of their composition and structure. The results are compiled in Fig. 3a,b. The intense XRD peaks (Fig. 3a) at $2\theta = 25.4^\circ$ and 27.6° can be assigned to TiO_2 (101) anatase and (110) rutile reflections [43,44], respectively, while peaks at $2\theta \sim 23$ –24° can be ascribed to the monoclinic WO_3 phase [45]. The relatively intense reflections at $2\theta \sim 23$ –24° observed for the structure 1Pt-30 WO_3 - TiO_2 is well in line with the larger amount of sputtered W metal (additional XRD patterns are shown in Fig. S2). In any case, no XRD signal for Pt can be seen, owing to the small amount of sputtered noble metal.

The TEM images in Fig. 3b clearly show the decoration of the top of the tubes with the two cocatalyst (i.e. Pt and WO_3). The HR-TEM images (insets in Fig. 3b) reveal the presence of both anatase TiO_2 (101)

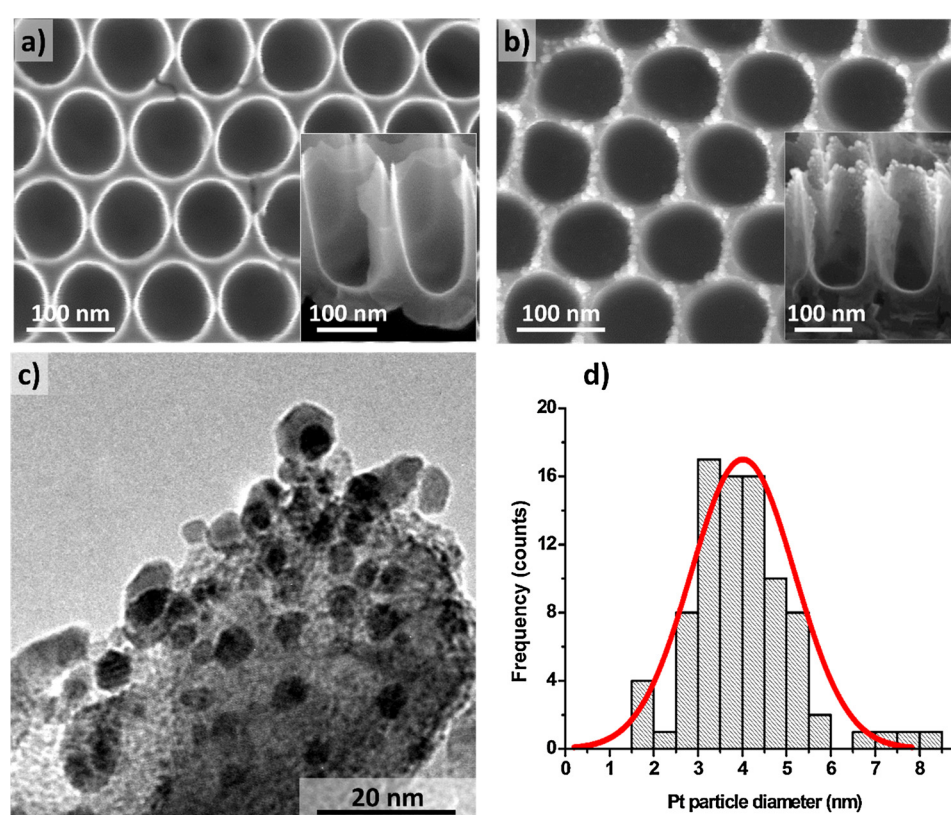


Fig. 1. (a–b) SEM images of various TiO_2 structures: (a) arrays of pristine TiO_2 nanotubes. Inset: cross-sectional view of the pristine NTs; (b) TiO_2 NTs coated with a sputtered 1 nm-thick Pt film after dewetting (thermal treatment at 450 °C, air, 1 h). Inset: cross sectional view. (c) TEM image of the very top of a nanotube decorated with a sputtered-dewetted 1 nm-thick Pt film; (d) Pt NP size distribution.

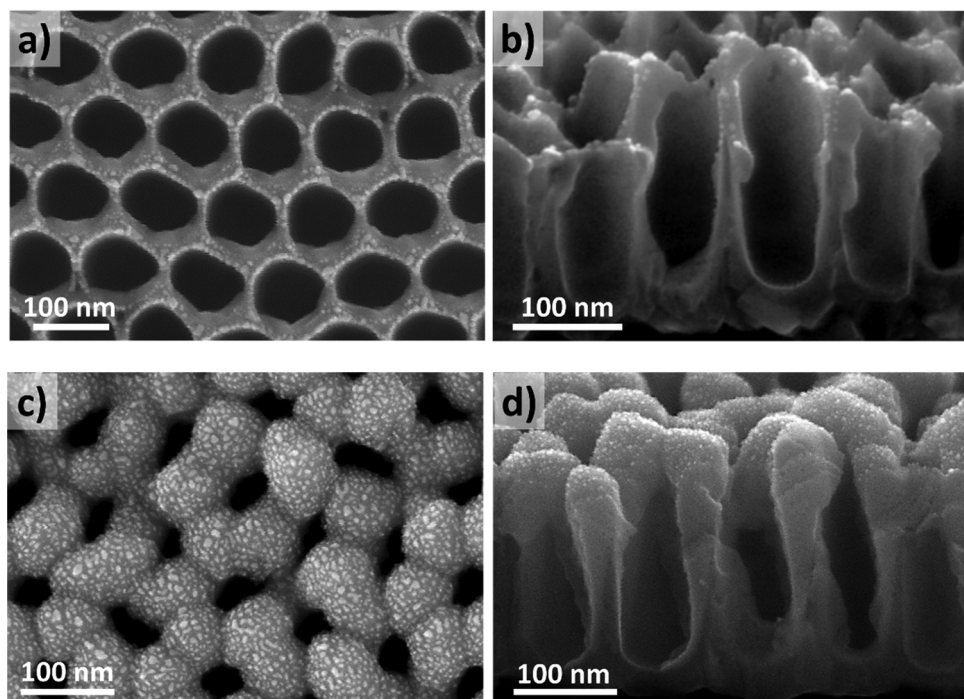


Fig. 2. (a, c) Top and (b, d) cross sectional SEM images of TiO_2 NTs coated with (a, b) 5 nm-thick and (c, d) 30 nm-thick W film and then with Pt (1 nm-thick). All the structures were subjected to thermal treatment and dewetting.

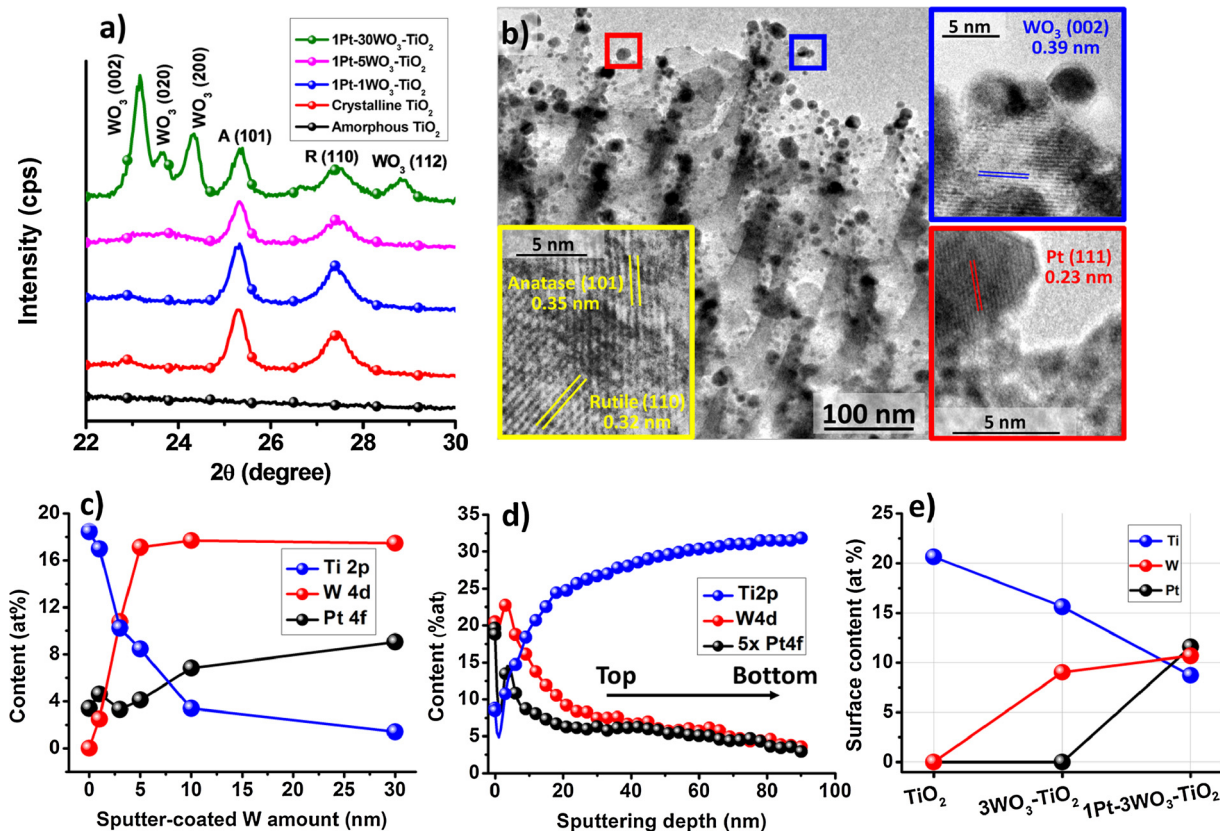


Fig. 3. (a) Magnified view of the XRD patterns showing the main reflections of anatase (A) and rutile (R) TiO_2 and monoclinic WO_3 , (XRD patterns measured in the 20–80° 2 θ range are in Fig. S2). (b) TEM images of sample 1Pt-5WO₃-TiO₂. Insets: HR-TEM images: (yellow) crystal planes of (101) anatase TiO_2 and (110) rutile TiO_2 in the sidewalls and bottom of the nanotubes; (blue) crystal planes of (002) monoclinic WO_3 and (red) crystal planes of (111) cubic Pt at the very top of the nanotubes. (c,d and e) Ti, W and Pt content determined from XPS analysis: (c) surface content as a function of the nominal thickness of the sputter-coated W films, (d) depth profile (content measured along the depth of the nanotubes; the Pt signal in the plot is magnified by a factor 5x) and (e) Ti, W and Pt surface content of three differently decorated TiO_2 NT layers showing the change in surface composition after the different steps of the W and Pt sputter deposition approach and thermal treatment (For interpretation of the references to colour in this figure legend, the reader is referred to the web version of this article).

and rutile TiO_2 (110) in the sidewalls and bottoms of the tubes, and, confirm the site-selective placement of the monoclinic WO_3 layer and Pt NPs on the top of the tubes. For example, the HR-TEM image in the blue box in Fig. 3b clearly shows the WO_3 lattice planes – in the same image one can also identify, owing to a clearly different contrast, various Pt nanoparticles of a size distribution that is in line with that shown in Fig. 1d. Thus, SEM analysis along with XRD and TEM results (as well as XPS data below) confirm the presence of Pt nanoparticles as well as the conversion of the sputtered W metal to crystalline WO_3 layer atop the architecture.

XPS analysis was carried out to investigate the composition of these structures and to gain information of the interfaces constructed in the $\text{Pt}/\text{WO}_3/\text{TiO}_2$ cocatalytic stack. The XPS surveys (Fig. S3a) show that the structures are composed of Ti, O, W and Pt, with small traces of adventitious carbon and P (due to the anodization in highly-concentrated $\text{o-H}_3\text{PO}_4$). The XPS doublet with signals peaking at ~ 71.3 and 74.7 eV (Fig. S3b) can be assigned to $\text{Pt}4\text{f}_{7/2}$ and $\text{Pt}4\text{f}_{5/2}$, respectively [46], and confirms the metallic state of the dewetted Pt nanoparticles. The XPS doublet peaking at ~ 36.5 and 38.7 eV (Fig. S3c) can be attributed to WO_3 [47,48]. Note that in contrast to what is observed for Pt (i.e. solid-state thermal dewetting leading to rupture of the Pt film into Pt NPs), the sputter-coated W film is subjected to a different fate when annealed in air: it reacts with O_2 gas (thermal oxidation) and forms a crystalline WO_3 layer atop the NTs [49].

The XPS data reported in Fig. 3c show that the $\text{Ti}2\text{p}$ signal for the NT structures decreases with increasing the amount of sputtered W. This is well in line with data in Fig. S3d, and indicates that the WO_3 layers formed from W sputtered films > 10 nm cover almost totally the TiO_2 NT surface. The weak Ti signal is in this case attributed to the uncovered TiO_2 surface at the very bottom of the tubes. A side effect of sputter-coating W film > 5 nm is the increase of the surface content of Pt at the top of the structures. This can be ascribed to the narrowing of the tube mouth (as clearly shown in Fig. 2c and d). Hence, the relatively large amount of deposited W makes available a larger surface on the top of the cavities for Pt deposition.

The XPS depth profiling (Fig. 3d) corroborates the stacked architecture of the photocatalyst, with the presence of Pt and WO_3 only at the very top of the tubes, i.e. the signals of Pt and W decrease sharply from the NT top towards the bottom of the cavities.

The XPS data in Fig. 3e show the change in surface composition after each step of sputter-deposition and thermal treatment, i.e. in order to form the structures $3\text{WO}_3\text{-TiO}_2$ and $1\text{Pt- WO}_3\text{-TiO}_2$. The Ti signal drops significantly after the sequential W and Pt sputter coating, confirming that the WO_3 layer firstly and then the Pt nanoparticles are deposited atop the TiO_2 nanotubes. Moreover, the amount of W in $1\text{Pt-WO}_3\text{-TiO}_2$ and $\text{WO}_3\text{-TiO}_2$ is comparable, which confirms not only the reliability of the cocatalyst deposition method (fine control over amount and placement), but also that Pt cocatalyst is deposited atop the nanotube structure. The atomic concentration of the various elements in the structures are summarized in Table S1.

In order to evaluate the interaction of Pt, WO_3 and TiO_2 with each other at the different formed interfaces, the high resolution XPS spectra in the W4f and Pt4f regions for different structures (TiO_2 , Pt-TiO_2 , $\text{WO}_3\text{-TiO}_2$ and $\text{Pt-WO}_3\text{-TiO}_2$) are overlaid in Fig. S4a and b, respectively. The W state (Fig. S4a) is virtually identical in $\text{WO}_3\text{-TiO}_2$ and $\text{Pt-WO}_3\text{-TiO}_2$. The peak at 36.48 eV observed for pristine TiO_2 is ascribe to the $\text{Ti}3\text{p}$ signal, which falls in the W4f signal region. Also, as it is evident from Fig. S4b, Pt is present in its metallic form, and no shift could be detected in the Pt4f doublets of Pt-TiO_2 and $\text{Pt-WO}_3\text{-TiO}_2$ structures. In other words, the XPS data confirm the stacked architecture of the Pt-WO_3 cocatalyst atop the NTs, and the sequential deposition of the WO_3 and Pt cocatalytic elements does not affect their chemical state, which is for each element comparable in the different structures.

These structures were assessed in view of their photocatalytic H_2 evolution performance, from water-ethanol (20%) solution under UV light irradiation (LED light, 365 nm). The results are shown in Fig. 4a–c.

From these data it is clear that, for these stacked structures, an optimized amount of sputtered W leads to significantly higher photocatalytic H_2 generation efficiency than any other combination (Pt-TiO_2 , $\text{WO}_3\text{-TiO}_2$) or pristine TiO_2 . More precisely, both pristine TiO_2 NTs (TiO_2) and TiO_2 NTs modified only with WO_3 ($3\text{WO}_3\text{-TiO}_2$) exhibit a negligible photocatalytic H_2 generation ($0.06 \mu\text{L h}^{-1} \text{cm}^{-2}$ and $0.14 \mu\text{L h}^{-1} \text{cm}^{-2}$, respectively). The slight improvement of the r_{H_2} may be ascribed to electron-hole separation at the TiO_2/WO_3 interface, which can make electrons more available for the H_2 evolution (spatially separated charges). As expected, Pt-TiO_2 photocatalyst (1Pt-TiO_2) shows an improved H_2 evolution compared to pristine TiO_2 , i.e. leading to a r_{H_2} of $3.4 \mu\text{L h}^{-1} \text{cm}^{-2}$. This effect is due to the formation of Pt/TiO_2 Schottky junctions at the TiO_2 nanotubes top.

Nevertheless, a substantial further enhancement of the photocatalytic performance is obtained modifying TiO_2 with both WO_3 and Pt ($1\text{Pt-xWO}_3\text{-TiO}_2$), that is, by constructing a stacked $\text{Pt-WO}_3\text{-TiO}_2$ architecture at the NT top. In particular, photocatalysts with 1 , 3 and 5 nm of WO_3 lead to the highest H_2 generation rates, that is, of 4.4 , 5.0 and $5.2 \mu\text{L h}^{-1} \text{cm}^{-2}$, respectively. Note that these r_{H_2} can be up to a factor 1.5 higher than that of 1Pt-TiO_2 . Long-run photocatalytic tests (carried out by continuous irradiation for 30 h – Fig. 4c) reveal that the r_{H_2} remains constant and thus, deterioration phenomena such as photo-corrosion of the photocatalyst or fall-off of the cocatalytic Pt NPs can be ruled out.

Taking into account the band edge alignment and energetic situation of the elements of the $\text{Pt-WO}_3\text{-TiO}_2$ triad, one can interpret these photocatalytic results assuming that the defined $\text{Pt-WO}_3\text{-TiO}_2$ architecture constructed at the top of the NT walls enables efficient electron transfer from the TiO_2 NTs (light absorber and charge carrier generator) to the WO_3 top layer, and then onward to the Pt cocatalytic NPs. This “electron transfer cascade” is therefore the main cause for the observed synergistic r_{H_2} enhancement.

A side effect of the site-selective decoration of the NT top only (W films < 10 nm) is that the bottom of the TiO_2 nanocavities is left uncoated, i.e. free TiO_2 surface. This situation, along with the intrinsic upward band bending in the nanotube walls [50] and the typically short diffusion length of holes in TiO_2 , leads to direct hole-transfer to the reactants (ethanol), which reduced the electron-hole recombination in the NTs.

In order to corroborate the results of photocatalytic H_2 evolution and their interpretation, photo-degradation tests of Acid Orange 7 (AO7) under 365 nm UV light irradiation were carried out with the reference materials 1Pt-TiO_2 and $3\text{WO}_3\text{-TiO}_2$, and different three-layered structures, i.e., $1\text{Pt-3WO}_3\text{-TiO}_2$ and $1\text{Pt-30WO}_3\text{-TiO}_2$. The results are reported in Fig. 4d and e. Noteworthy, also in this case, for single-cocatalyst structures, the deposition of a noble metal (1Pt-TiO_2) leads to a significantly higher AO7 photocatalytic degradation rate compared to the modification with WO_3 ($\text{WO}_3\text{-TiO}_2$). More importantly, the $\text{Pt-WO}_3\text{-TiO}_2$ triad with optimized amount of W ($\sim 1\text{--}5$ nm) leads to a higher photocatalytic performance (AO7 degradation) compared to 1Pt-TiO_2 . However, a too large amount of W (~ 30 nm) leads to a lower AO7 degradation rate. In other words, these data are fully in line with the H_2 evolution results.

In order to understand the role of the WO_3 top layer and of the thickness on the photocatalytic performance, the light absorption properties of the different structures along with their photo-electrochemical behavior were investigated by measuring UV-vis diffuse reflectance (DR UV-vis) and photocurrent spectra (see Figs. 5 and S5, respectively). Interestingly, only minor differences in terms of light absorbance between the various morphologies were observed at 365 nm (Fig. 5). Besides, the photocurrent trend observed in the photo-electrochemical measurements is: $\text{TiO}_2 > 3\text{WO}_3\text{-TiO}_2 > 1\text{Pt-3WO}_3\text{-TiO}_2 > 1\text{Pt-TiO}_2$ (Fig. S5). In other words, in a photo-electrochemical configuration, photo-anodes consisting of pristine nanotube arrays outperform any other cocatalyst-decorated structures (additional discussion is given in the supplementary information). Also, a virtually

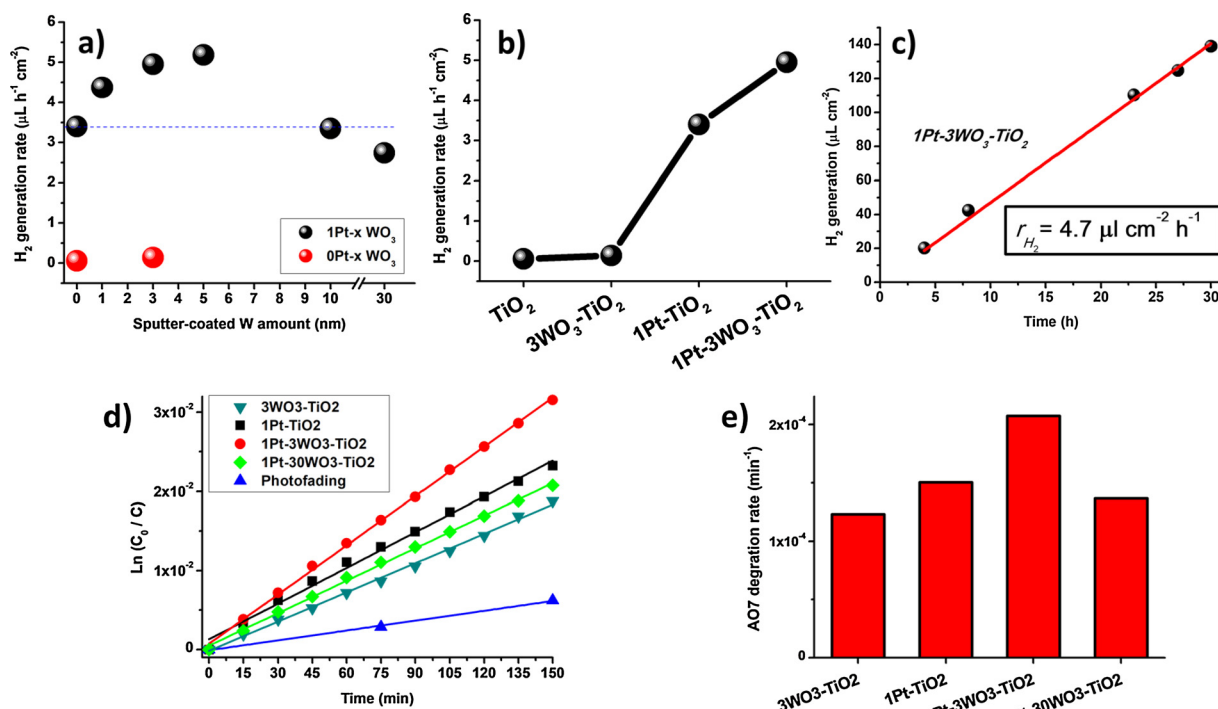


Fig. 4. (a) Photocatalytic H₂ evolution results of different TiO₂ nanotube structures as a function of sputtered W amount; (b) summary of the r_{H_2} improvement achieved with an optimized Pt and WO₃ decoration on the top of the TiO₂ NT arrays. (c) Evaluation of the photocatalytic H₂ evolution performance of 1Pt-3WO₃-TiO₂ over an irradiation time of 30 h. (d) First-order kinetic fitting for the photocatalytic degradation (oxidation) of AO7 (Acid Orange 7) using different TiO₂ nanotube structures. (e) AO7 degradation rates for the different samples.

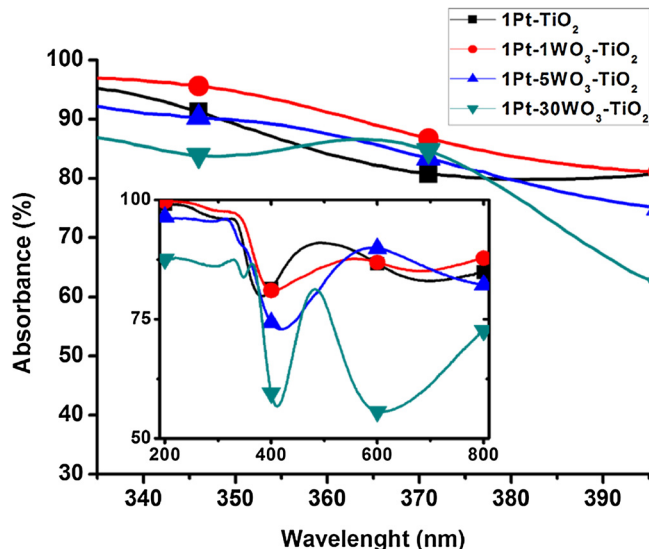


Fig. 5. Detail of the DR UV-vis spectra of different TiO₂ structures in the region around 365 nm (i.e. wavelength used in this work for the photocatalytic experiments). Inset: DR UV-vis spectra measured in the 200–800 nm wavelength range.

identical bandgap of 3.0 eV can be estimated for the various structures, which is in line with that of anatase TiO₂.

Considering these results, it is clear that the light harvesting ability of the different structures (i.e. different W loadings) does not have a dominant effect on the photocatalytic performance – here, it is reasonable to assume that WO₃ is not the photoactive material in this photocatalytic architecture, but acts as a buffer (transfer) layer for TiO₂ electrons, and the contribution of charges generated directly in WO₃ to H₂ evolution may be negligible.

Thus, one can assume that the Pt-WO₃-TiO₂ structure is properly constructed only when the WO₃ top layer is sufficiently thin: in this case it can favor charge carrier separation by electron transfer towards the top of the tube, through the WO₃ buffer layer, and then onward to the Pt NPs for H₂ evolution. The energetic situation was confirmed by XPS valence band measurements (Fig. S6) that show similar valence band maxima for both TiO₂ (nanotubes) and WO₃ (buffer layer) – that is, the WO₃ CB minimum lies in this photocatalytic architecture above the redox potential of water, as illustrated in Fig. 6.

In this construction, crucial is also the uncoated bottom of the TiO₂ cavities that allows for direct hole-transfer to the reaction phase (hole-scavenging). This explains also the low H₂ yield of the sample 1Pt-30WO₃-TiO₂, that is, a too thick WO₃ buffer layer not only blocks TiO₂ hole-transfer to the environment at the tube bottom, but also can make less efficient the electron transport across the WO₃ layer owing to an increased charge transfer resistance. These findings are in line with the

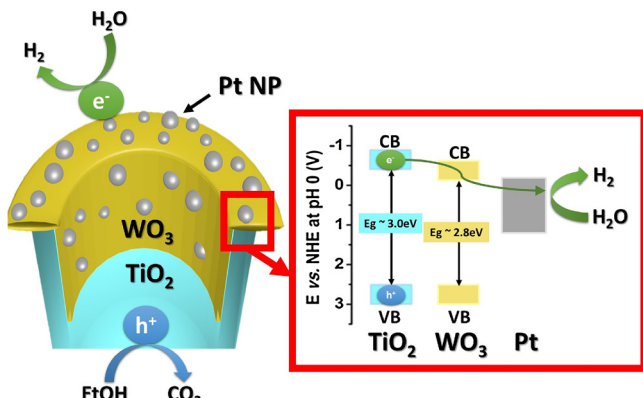


Fig. 6. Scheme of the structure of the three-layered photocatalyst illustrating the band alignment (TiO₂-WO₃ [51] energetic situation) that allows for the proposed mechanism of electron transfer cascade.

proposed electron transfer cascade mechanism, and well support EIS results obtained for similar stacked-architectures [13] for which charge accumulation can be observed in $\text{WO}_3\text{-TiO}_2$ structures under UV light illumination (TiO_2 CB electrons are transferred to WO_3), while the accumulated charge is depleted when Pt nanoparticles are decorated atop the WO_3 buffer layer (in the Pt- $\text{WO}_3\text{-TiO}_2$ architecture electrons are extracted by Pt and transferred to the environment for H_2 evolution).

4. Conclusions

We introduced the fabrication of an efficient photocatalytic platform based on an electron transfer cascade mechanism designed by site-selective decoration of the top of highly-ordered TiO_2 nanotubes with a well-defined Pt- WO_3 cocatalyst stack. We show that a morphological control with nanoscale precision of the cocatalyst-catalyst structure not only allows for a systematic assessment of the charge carrier dynamics and photocatalytic mechanism, but also is key to design functional composite architectures that can achieve strongly enhanced photocatalytic H_2 evolution efficiencies.

Acknowledgements

The authors would like to acknowledge ERC (340511), DFG and the DFG cluster of excellence EAM (EXC 315) for financial support, as well as H. Hildebrand, S. Hejazi, and N.T. Nguyen for valuable discussion and technical help. D.S. and S.R. gratefully acknowledge financial support from MIUR.

Appendix A. Supplementary data

Supplementary material related to this article can be found, in the online version, at doi:<https://doi.org/10.1016/j.apcatb.2018.05.061>.

References

- A. Fujishima, K. Honda, Electrochemical photolysis of Water at a semiconductor electrode, *Nature* 238 (1972) 37–38, <http://dx.doi.org/10.1038/238037a0>.
- P. Roy, S. Berger, P. Schmuki, TiO_2 nanotubes: synthesis and applications, *Angew. Chem. Int. Ed.* 50 (2011) 2904–2939, <http://dx.doi.org/10.1002/anie.201001374>.
- K. Lee, A. Mazare, P. Schmuki, One-dimensional titanium dioxide nanomaterials: nanotubes, *Chem. Rev.* 114 (2014) 9385–9454, <http://dx.doi.org/10.1021/cr500061m>.
- I. Paramasivam, H. Jha, N. Liu, P. Schmuki, A review of photocatalysis using self-organized TiO_2 nanotubes and other ordered oxide nanostructures, *Small* 8 (2012) 3073–3103, <http://dx.doi.org/10.1002/smll.201200564>.
- M. Assefpour-Dezfuly, C. Vlachos, E.H. Andrews, Oxide morphology and adhesive bonding on titanium surfaces, *J. Mater. Sci.* 19 (1984) 3626–3639, <http://dx.doi.org/10.1007/BF02396935>.
- V. Zwilling, M. Aucourier, E. Darque-Ceretti, Anodic oxidation of titanium and $\text{TA}6\text{V}$ alloy in chromic media. An electrochemical approach, *Electrochim. Acta* 45 (1999) 921–929, [http://dx.doi.org/10.1016/S0013-4686\(99\)00283-2](http://dx.doi.org/10.1016/S0013-4686(99)00283-2).
- M. Ge, C. Cao, J. Huang, S. Li, Z. Chen, K.-Q. Zhang, S.S. Al-Deyab, Y. Lai, A review of one-dimensional TiO_2 nanostructured materials for environmental and energy applications, *J. Mater. Chem. A* 4 (2016) 6772–6801, <http://dx.doi.org/10.1039/C5TA09323F>.
- F. Riboni, N.T. Nguyen, S. So, P. Schmuki, Aligned metal oxide nanotube arrays: key-aspects of anodic TiO_2 nanotube formation and properties, *Nanoscale Horiz.* 1 (2016) 445–466, <http://dx.doi.org/10.1039/C6NH00054A>.
- D. Kowalski, D. Kim, P. Schmuki, TiO_2 nanotubes, nanochannels and mesoporous: Self-organized formation and applications, *Nano Today* 8 (2013) 235–264, <http://dx.doi.org/10.1016/j.nantod.2013.04.010>.
- X. Feng, K. Shankar, O.K. Varghese, M. Paulose, T.J. Latempa, C.A. Grimes, Vertically aligned single crystal TiO_2 nanowire arrays grown directly on transparent conducting oxide coated glass: synthesis details and applications, *Nano Lett.* 8 (2008) 3781–3786, <http://dx.doi.org/10.1021/nl802096a>.
- M.A. Butler, Photoelectrolysis and physical properties of the semiconducting electrode WO_2 , *J. Appl. Phys.* 48 (1977) 1914–1920, <http://dx.doi.org/10.1063/1.323948>.
- W. Gissler, Photoelectrochemical processes at semiconducting $\text{WO}_{[3]}$ layers, *J. Electrochem. Soc.* 124 (1977) 1710, <http://dx.doi.org/10.1149/1.2133141>.
- M. Altomare, N.T. Nguyen, S. Hejazi, P. Schmuki, A cocatalytic electron-transfer Cascade site-selectively placed on TiO_2 nanotubes yields enhanced photocatalytic H_2 evolution, *Adv. Funct. Mater.* 28 (2018) 1–9, <http://dx.doi.org/10.1002/adfm.201704259>.
- A. Benoit, I. Paramasivam, Y.-C. Nah, P. Roy, P. Schmuki, Decoration of TiO_2 nanotube layers with WO_3 nanocrystals for high-electrochromic activity, *Electrochem. Commun.* 11 (2009) 728–732, <http://dx.doi.org/10.1016/j.elecom.2009.01.024>.
- A.O.T. Patrocínio, L.F. Paula, R.M. Paniago, J. Freitag, D.W. Bahnenmann, layer-by-layer $\text{TiO}_2\text{/WO}_3$ thin films As efficient photocatalytic self-cleaning surfaces, *ACS Appl. Mater. Interfaces* 6 (2014) 16859–16866, <http://dx.doi.org/10.1021/am504269a>.
- F. Riboni, L.G. Bettini, D.W. Bahnenmann, E. Sellì, $\text{WO}_3\text{-TiO}_2$ vs. TiO_2 photocatalysts: effect of the W precursor and amount on the photocatalytic activity of mixed oxides, *Catal. Today* 209 (2013) 28–34, <http://dx.doi.org/10.1016/j.cattod.2013.01.008>.
- F. Riboni, M.V. Dozzi, M.C. Paganini, E. Giamello, E. Sellì, Photocatalytic activity of $\text{TiO}_2\text{-WO}_3$ mixed oxides in formic acid oxidation, *Catal. Today* 287 (2017) 176–181, <http://dx.doi.org/10.1016/j.cattod.2016.12.031>.
- A. Fuerte, M.D. Hernández-Alonso, A.J. Maira, A. Martínez-Arias, M. Fernández-García, J.C. Conesa, J. Soria, G. Munuera, Nanosize Ti-W mixed oxides: effect of doping level in the photocatalytic degradation of toluene using sunlight-type excitation, *J. Catal.* 212 (2002) 1–9, <http://dx.doi.org/10.1006/jcat.2002.3760>.
- M.M. Momeni, Y. Ghayeb, Fabrication, characterization and photocatalytic properties of $\text{Au/TiO}_2\text{-WO}_3$ nanotubular composite synthesized by photo-assisted deposition and electrochemical anodizing methods, *J. Mol. Catal. A Chem.* 417 (2016) 107–115, <http://dx.doi.org/10.1016/j.molcata.2016.03.024>.
- J. Papp, S. Soled, K. Dwight, A. Wold, Surface acidity and photocatalytic activity of TiO_2 , $\text{WO}_3\text{/TiO}_2$, and $\text{MoO}_3\text{/TiO}_2$ photocatalysts, *Chem. Mater.* 6 (1994) 496–500, <http://dx.doi.org/10.1021/cm00040a026>.
- Y. Tae Kwon, K. Yong Song, W.In Lee, G. Jin Choi, Y. Rag Do, Photocatalytic behavior of WO_3 -loaded TiO_2 in an oxidation reaction, *J. Catal.* 191 (2000) 192–199, <http://dx.doi.org/10.1006/jcat.1999.2776>.
- V. Keller, Photocatalytic oxidation of butyl acetate in vapor phase on TiO_2 , Pt/TiO_2 and $\text{WO}_3\text{/TiO}_2$ catalysts, *J. Catal.* 215 (2003) 129–138, [http://dx.doi.org/10.1016/S0021-9517\(03\)00002-2](http://dx.doi.org/10.1016/S0021-9517(03)00002-2).
- J.H. Pan, W.I. Lee, Preparation of highly ordered cubic mesoporous WO_3 / TiO_2 films and their photocatalytic properties, *Chem. Mater.* 18 (2006) 847–853, <http://dx.doi.org/10.1021/cm0522782>.
- K.K. Akurati, A. Vital, J. Dellemann, K. Michalow, T. Graule, D. Ferri, A. Baiker, Flame-made $\text{WO}_3\text{/TiO}_2$ nanoparticles: relation between surface acidity, structure and photocatalytic activity, *Appl. Catal. B Environ.* 79 (2008) 53–62, <http://dx.doi.org/10.1016/j.apcatb.2007.09.036>.
- M. Carrus, M. Fantauzzi, F. Riboni, M. Makosch, A. Rossi, E. Sellì, J.A. van Bokhoven, Increased conversion and selectivity of 4-nitrostyrene hydrogenation to 4-aminostyrene on Pt nanoparticles supported on titanium-tungsten mixed oxides, *Appl. Catal. A Gen.* 519 (2016) 130–138, <http://dx.doi.org/10.1016/j.apcata.2016.03.031>.
- K.Y. Song, M.K. Park, Y.T. Kwon, H.W. Lee, W.J. Chung, W.I. Lee, Preparation of transparent particulate MoO_3 / TiO_2 and WO_3 / TiO_2 films and their photocatalytic properties, *Chem. Mater.* 13 (2001) 2349–2355, <http://dx.doi.org/10.1021/cm000858n>.
- H. Gao, P. Zhang, J. Hu, J. Pan, J. Fan, Applied surface science one-dimensional Z-scheme TiO_2 / WO_3 / Pt heterostructures for enhanced hydrogen generation, *Appl. Surf. Sci.* 391 (2017) 211–217, <http://dx.doi.org/10.1016/j.apsusc.2016.06.170>.
- N.T. Nguyen, M. Altomare, J.E. Yoo, N. Taccardi, P. Schmuki, Noble metals on anodic TiO_2 nanotube mouths: thermal dewetting of minimal Pt co-catalyst loading leads to significantly enhanced photocatalytic H_2 generation, *Adv. Energy Mater.* 6 (2016) 1501926, <http://dx.doi.org/10.1002/aenm.201501926>.
- J. Yoo, M. Altomare, M. Mokhtar, A. Alshehri, S.A. Al-Thabaiti, A. Mazare, P. Schmuki, Photocatalytic H_2 generation using dewetted Pt-decorated TiO_2 nanotubes: optimized dewetting and oxide crystallization by a multiple annealing process, *J. Phys. Chem. C* 120 (2016) 15884–15892, <http://dx.doi.org/10.1021/acs.jpcc.5b12050>.
- N.T. Nguyen, J. Yoo, M. Altomare, P. Schmuki, Suspended” Pt nanoparticles over TiO_2 nanotubes for enhanced photocatalytic H_2 evolution, *Chem. Commun.* 50 (2014) 9653–9656, <http://dx.doi.org/10.1039/C4CC04087B>.
- G.R. Bamwenda, S. Tsubota, T. Nakamura, M. Haruta, Photoassisted hydrogen production from a water-ethanol solution: a comparison of activities of Au-TiO_2 and Pt-TiO_2 , *J. Photochem. Photobiol. A Chem.* 89 (1995) 177–189, [http://dx.doi.org/10.1016/10.1016-6030\(95\)04039-I](http://dx.doi.org/10.1016/10.1016-6030(95)04039-I).
- A. Naldoni, M. D'Arienzo, M. Altomare, M. Marelli, R. Scotti, F. Morazzoni, E. Sellì, V. Dal Santo, Pt and Au/TiO_2 photocatalysts for methanol reforming: role of metal nanoparticles in tuning charge trapping properties and photoefficiency, *Appl. Catal. B Environ.* 130–131 (2013) 239–248, <http://dx.doi.org/10.1016/j.apcatb.2012.11.006>.
- G.L. Chiarello, M.H. Aguirre, E. Sellì, Hydrogen production by photocatalytic steam reforming of methanol on noble metal-modified TiO_2 , *J. Catal.* 273 (2010) 182–190, <http://dx.doi.org/10.1016/j.jcat.2010.05.012>.
- Z. Liu, Y. Lu, L. Yuan, L. Ma, L. Zheng, J. Zhang, T. Hu, Selective catalytic reduction of NO_x with H_2 over WO_3 promoted Pt/TiO_2 catalyst, *Appl. Catal. B Environ.* 188 (2016) 189–197, <http://dx.doi.org/10.1016/j.apcatb.2016.02.008>.
- É. Karácsonyi, L. Baia, A. Dombi, V. Danciu, K. Mogyorósi, L.C. Pop, G. Kovács, V. Coșevanu, A. Vulpoi, S. Simon, Z. Pap, The photocatalytic activity of TiO_2 / WO_3 /noble metal (Au or Pt) nanoarchitectures obtained by selective photo-deposition, *Catal. Today* 208 (2013) 19–27, <http://dx.doi.org/10.1016/j.cattod.2012.09.038>.
- G. Kovács, L. Baia, A. Vulpoi, T. Radu, É. Karácsonyi, A. Dombi, K. Hernádi, V. Danciu, S. Simon, Z. Pap, Applied catalysis *TiO* *2* / *WO* *3* / *Au* nanoarchitectures' photocatalytic activity, “from degradation intermediates to

catalysts' structural peculiarities", part I : aerioxide P25 based composites, *Applied Catal. B, Environ.* 147 (2014) 508–517, <http://dx.doi.org/10.1016/j.apcatb.2013.09.019>.

[37] M. Rusu, M. Baia, Z. Pap, V. Danciu, L. Baia, Structural investigations of TiO₂–WO₃–Au porous composites, *J. Mol. Struct.* 1073 (2014) 150–156, <http://dx.doi.org/10.1016/j.molstruc.2014.04.087>.

[38] L. Baia, A. Vulpoi, T. Radu, É. Karácsonyi, A. Dombi, K. Hernádi, V. Danciu, S. Simon, K. Norén, S.E. Canton, G. Kovács, Z. Pap, TiO₂/WO₃/Au nanoarchitectures' photocatalytic activity "from degradation intermediates to catalysts' structural peculiarities" part II: aerogel based composites – fine details by spectroscopic means, *Appl. Catal. B Environ.* 148–149 (2014) 589–600, <http://dx.doi.org/10.1016/j.apcatb.2013.12.034>.

[39] J.E. Yoo, K. Lee, M. Altomare, E. Sellì, P. Schmuki, Self-organized arrays of single-metal catalyst particles in TiO₂ cavities: a highly efficient photocatalytic system, *Angew. Chem. Int. Ed.* 52 (2013) 7514–7517, <http://dx.doi.org/10.1002/anie.201302525>.

[40] G. Cha, M. Altomare, N. Truong Nguyen, N. Taccardi, K. Lee, P. Schmuki, Double-Side Co-catalytic activation of anodic TiO₂ nanotube membranes with sputter-Coated Pt for photocatalytic H₂ generation from Water/Methanol mixtures, *Chem. Asian J.* 12 (2017) 314–323, <http://dx.doi.org/10.1002/asia.201601356>.

[41] C.V. Thompson, Solid-State dewetting of thin films, *Annu. Rev. Mater. Res.* 42 (2012) 399–434, <http://dx.doi.org/10.1146/annurev-matsci-070511-155048>.

[42] M. Altomare, N.T. Nguyen, P. Schmuki, Templated dewetting: designing entirely self-organized platforms for photocatalysis, *Chem. Sci.* 7 (2016) 6865–6886, <http://dx.doi.org/10.1039/C6SC02555B>.

[43] M. Liu, L. Piao, L. Zhao, S. Ju, Z. Yan, T. He, C. Zhou, W. Wang, Anatase TiO₂ single crystals with exposed {001} and {110} facets: facile synthesis and enhanced photocatalysis, *Chem. Commun.* 46 (2010) 1664, <http://dx.doi.org/10.1039/b924172h>.

[44] B. Liu, E.S. Aydil, Growth of oriented single-crystalline rutile TiO₂ nanorods on transparent conducting substrates for dye-sensitized solar cells, *J. Am. Chem. Soc.* 131 (2009) 3985–3990, <http://dx.doi.org/10.1021/ja8078972>.

[45] M. Righetto, S.E. Pratsinis, Annealing dynamics of WO₃ by *in situ* XRD, *Mater. Res. Bull.* 59 (2014) 199–204, <http://dx.doi.org/10.1016/j.materresbull.2014.07.018>.

[46] K.S. Kim, N. Winograd, R.E. Davis, Electron spectroscopy of platinum-oxygen surfaces and application to electrochemical studies, *J. Am. Chem. Soc.* 93 (1971) 6296–6297, <http://dx.doi.org/10.1021/ja00752a065>.

[47] B.O. Loopstra, H.M. Rietveld, Further refinement of the structure of WO₃, *Acta Crystallogr. Sect. B Struct. Cryst. Chem.* 25 (1969) 1420–1421, <http://dx.doi.org/10.1107/S0567740869004146>.

[48] M. Altomare, O. Pfoch, A. Tighineanu, R. Kirchgeorg, K. Lee, E. Sellì, P. Schmuki, Molten o-H₃PO₄ : a New electrolyte for the anodic synthesis of self-organized oxide structures – WO₃ nanochannel layers and others, *J. Am. Chem. Soc.* 137 (2015) 5646–5649, <http://dx.doi.org/10.1021/jacs.5b02104>.

[49] A. Herz, A. Franz, F. Theska, M. Hentschel, T. Kups, D. Wang, P. Schaaf, Solid-state dewetting of single- and bilayer Au-W thin films: unraveling the role of individual layer thickness, stacking sequence and oxidation on morphology evolution, *AIP Adv.* 6 (2016) 35109, <http://dx.doi.org/10.1063/1.4944348>.

[50] H. Han, F. Riboni, F. Karlicky, S. Kment, A. Goswami, P. Sudhagar, J. Yoo, L. Wang, O. Tomanec, M. Petr, O. Haderka, C. Terashima, A. Fujishima, P. Schmuki, R. Zboril, α -Fe2O3/TiO₂ 3D hierarchical nanostructures for enhanced photoelectrochemical water splitting, *Nanoscale* 9 (2017) 134–142, <http://dx.doi.org/10.1039/C6NR06908H>.

[51] L. Weinhardt, M. Blum, M. Bär, C. Heske, B. Cole, B. Marsen, E.L. Miller, Electronic surface level positions of WO₃ thin films for photoelectrochemical hydrogen production, *J. Phys. Chem. C* 112 (2008) 3078–3082, <http://dx.doi.org/10.1021/jp7100286>.